Progress In Electromagnetics Research B, Vol. 42, 141–161, 2012

INVESTIGATION OF CAVITY REFLEX ANTENNA USING CIRCULAR PATCH TYPE FSS SUPERSTRATE

A. Kotnala*, P. Juyal, A. Mittal, and A. De

Department of Electronics & Communication Engineering, Ambedkar Institute for Advanced Communication Technologies & Research, India

Abstract—Cavity reflex antenna (CRA) employing a circular patch type FSS (Frequency Selective Surface) superstrate is investigated. Analysis in terms of gain, bandwidth (impedance and gain) and radiation pattern has been presented. The aim of this work was to study low profile CRA having very thin superstrate sizes. In this CRA a circular patch antenna is used as a feeding source. The circular patch type FSS possesses some unique properties favorable for thin superstrate sizes. In practice when the excitation source of the CRA is a probe-fed microstrip antenna with finite ground plane, substrate and superstrate, cross-polarization increases. In the presented design, the cross polar level has been reduced by choosing the optimum air gap and superstrate geometrical and electrical properties. A CRA with circular patch type FSS offers better performance both in terms of gain and impedance bandwidth for, thin superstrates ($0.008\lambda_0$) while giving a gain of 13 dBi and considerably reduced crosspolar level. The proposed antenna exhibit nearly equal E-plane and H-plane radiation pattern. Measurement results are provided to support the simulated results (by Ansoft HFSS). The circular patch type FSS is easy to fabricate and can be embedded into the host profile.

1. INTRODUCTION

The gain and directive pattern of planar printed antennas can be improved by placing the superstrate covers at a specific distance from the antenna [1, 2]. There are several configurations for the design of superstrate layer which have been attempted in past. This includes the use of simple dielectrics [3], electromagnetic band gap

Received 25 April 2012, Accepted 28 June 2012, Scheduled 2 July 2012
* Corresponding author: Abhay Kotnala (kotnala3@gmail.com).

structures [4], artificial magnetics [5] and highly reflective frequency selective surfaces (FSS) [6, 7]. The technique of using a highly reflective frequency selective surfaces (FSS) for directivity and gain enhancement has been proved quite effective [7–10]. Design of Rectangular patch type FSS superstrate has been reported with printed dipole as a source antenna [7]. A highly directive resonant cavity antenna have been proposed by using metal strip grating (MSG) superstrate [11]. Exhaustive simulation and experimental study has been carried out and high values of directivity and gain have been reported. Effect of superstrate height on gain of fabry perot cavity antenna has been presented [12]. Directivity and bandwidth enhancement in a wide band aperture coupled patch antenna operating in x-band have been reported with the use of optimum FSS superstrate design [13]. High gain planar antenna using optimized partially reflecting surfaces has been presented in [14]. A novel high gain microstrip patch antenna with partially reflective superstrate is presented, where an AMC is utilized as ground plane is presented in [15].

In this paper, circular patch type FSS has been used as a patch antenna superstrate. Motivation for using circular patch type FSS superstrate comes from the findings in this paper which shows that it provides high value of reflection coefficient for a wide frequency band thus making it wideband highly reflective superstrate. Also as compare to the rectangle patch type FSS it take a less area and hence provide compactness. Firstly, the effects of disc radius and spacing as well as the effects of different dielectric slab as support of FSS, on the radiation parameters of the antenna has been studied. The structure proposed here, consists of circular patch type FSS imprinted on the superstrate dielectric. These FSS structure can be of any shape and size which determines their nature of affecting the field in their vicinity. The patch type FSS has already been proposed but the effect of the size and spacing of the obstacles on the antenna parameters and radiated field were not taken into account. This has been incorporated in the paper taking into account circular disc type FSS. The effect of superstrate height on the cross polar level in both E and H plane has been investigated here. Gain vs. Frequency plots are provided by varying the superstrate height, superstrate thickness and supporting dielectric constant of FSS superstrate.

In the previous findings [7] it has been observed that the FSS superstrate size and CRA air-gap height have considerable impact on the input impedance behavior, such as shifting the resonant frequency and changing the level of return loss at the input port. But it is shown in this paper that using circular patch type FSS superstrate changing the air gap height or superstrate size produces a very small

change in the resonant frequency and input impedance characteristic but considerably affect the cross polar level. Thus aforementioned FSS superstrate can be used to minimize the cross polar level and improve polarization purity without compromising the other parameter of the antenna like impedance bandwidth, frequency of operation and gain. For patch type FSS superstrate varying air gap thicknesses, beam scans from broadside to 45 and further. For a scan angle beyond 60 an undesirable secondary beam appears, one way to avoid the secondary beam problem is to increase the substrate permittivity between the feed and superstrate layer. But using a circular FSS superstrate the gap height does not readily affect the scan angle of the pattern and does not produce secondary beam problem even with air gap.

2. ANTENNA MODELING

The proposed cavity reflex antenna employing a circular disc type FSS superstrate is shown in the Fig. 1. It consists of a simple circular patch antenna excited by a probe as the source for the CRA. A circular disc type FSS superstrate is placed at a height (L) from the source antenna structure. The spacing or the height (L) consisting of air gap, has been created by using Teflon rods for supporting the FSS superstrate. The Teflon rods do not affect the antenna performance as seen in the measurement results. The location of the source from the superstrate strongly influences the level of radiation from the structure, and hence has significant effect on the input resistance or conductance as seen at the feed terminals. The source (planar circular patch antenna) and FSS design procedure is described below.

2.1. Source Design (Probe Fed Circular Patch Antenna)

The source for the proposed design consists of a simple circular patch resonating at 10 GHz. The circular patch is designed on Rogers RT Duroid 5880 (tm) having a dielectric constant of $\varepsilon_{r1} = 2.2$ and loss tangent of 0.0009 and thickness $h_1 = 0.762$ mm ($0.025\lambda_0$). The radius of the probe fed patch is 5.63 mm. The antenna produces small impedance bandwidth due to thin substrate used.

Parameters	Substrate	Superstrate	Gap
Relative permittivity	ε_{r1}	ε_{r2}	ε_r
Relative Permeability	μ_{r1}	μ_{r2}	μ_r
Thickness	h_1	h_2	L

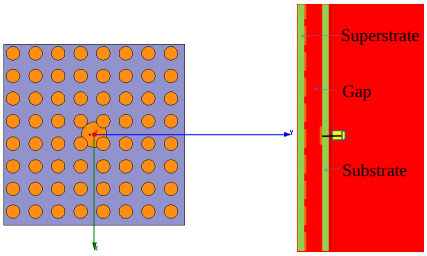

Figure 1. Top view of the cavity reflex antenna with disc type FSS superstrate (HFSS model).

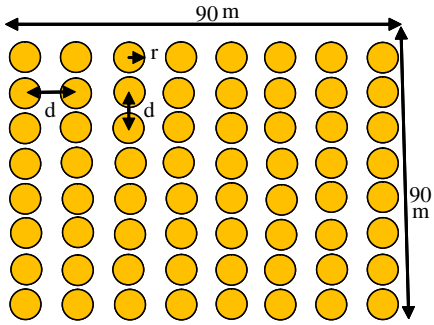

Figure 2. Enlarged view of the disc type FSS superstrate.

2.2. FSS Design and Modeling (Circular Disc Type FSS)

The key part of the antenna system is the highly reflective superstrate. The superstrate consist of periodic array of circular disc type structures formulated on PTFE slab (i.e., RT duroid dielectric 5880 of Rogers). The thickness of the superstrate $h_2 = 0.254\,\text{mm}$, i.e., $(0.008\lambda_0)$, is one third of the substrate height. This has been chosen to make the whole antenna a low profile structure. An enlarged top view of the FSS superstrate is shown in Fig. 2. The geometrical and electrical properties of the superstrate also affect the FSS response. This also affects the antenna performance and is shown later in this paper. The basic rule of design is to make the loop circumference approximately equal to the resonant wavelength. Though the disc dimensions need to be tuned to meet the desired frequency response as it affects the antenna performance. The period of repeating elements should be less than the shortest wavelength considered in the operating band for zero degree signal incidence. This is done to suppress the grating lobes. The spacing (L) between the source and FSS structure, in general, has material parameters characterized by permittivity and permeability. The gap has been filled by air in our case using spacers, however styro foam can also be used. The structure is usually excited by a single source located centrally and horizontally inside the parallel-plate region. In our case it is a circular patch antenna. In case of larger incidence angle the centre to centre spacing between the circular patches "d" as shown in the Fig. 2 should be kept less than one half of wavelength. This however just determines the starting value for design of FSS structure but the optimized design is obtain for the best performance of CRA antenna. The size of the FSS superstrate is

90 mm × 90 mm ($3\lambda_0 \times 3\lambda_0$) consisting of an 8×8 array of circular disc structures.

3. FULL WAVE ANALYSIS OF CRA EMPLOYING CIRCULAR DISC TYPE FSS

In this section the CRA using disc type FSS superstrate as proposed in Section 2 is analyzed using the commercial Electromagnetic simulation tool Ansoft HFSS based on FEM-CAD. The proposed FSS superstrate as shown in Fig. 1 is modeled in HFSS. The return loss and gain versus frequency plots are investigated for various parametric variations of geometrical and electrical properties of the FSS superstrate. This is done to obtain the optimum design and study the effects of superstrate parameters on performance. The effect of superstrate parameters, i.e., dielectric constant, size and space variation of the circular disc on gain and return loss of antenna are analyzed. The radiation pattern plot showing the cross polar and co-polar fields are shown for various combinations.

3.1. For simple Circular Patch

The simulated results of simple circular patch designed at 10 GHz are shown in Fig. 3. Return loss vs. frequency is shown in Fig. 3(a). The Impedance bandwidth (−10 dB) is 2.8%. The low impedance bandwidth is because of the use of very thin substrate of thickness 0.762 mm ($0.025\lambda_0$). The Figs. 3(b) and 3(c) shows the realized gain versus frequency and the radiation pattern of the simple antenna structure respectively. The patch antenna has a gain of 8.7 dBi in the broadside direction at the operating frequency and it ranges from 8.08 to 8.43 dBi in the antenna operating bandwidth range. The radiation pattern is distorted in the broadside direction with the maxima shifted by 15 degrees from the centre or the broadside. The gain bandwidth of the simple circular patch, which is defined as the frequency range where the gain drops 3 dB from its maximum, is 8.7%.

3.2. For CRA with Disc Type FSS Superstrate

The physics of directive beaming for CRA where the PRS acts like a leaky parallel plate waveguide [14] for $\lambda_d/2 < L < \lambda_d$ where $\lambda_d = \lambda_0/n_1$ is the wavelength inside the dielectric substrate filling the gap and hence only $n = 1$ pair of modes would be above cut off. In all cases, the thickness L of the substrate filling the gap directly controls the beam angle θ_0 and determines whether the beam is a broadside beam

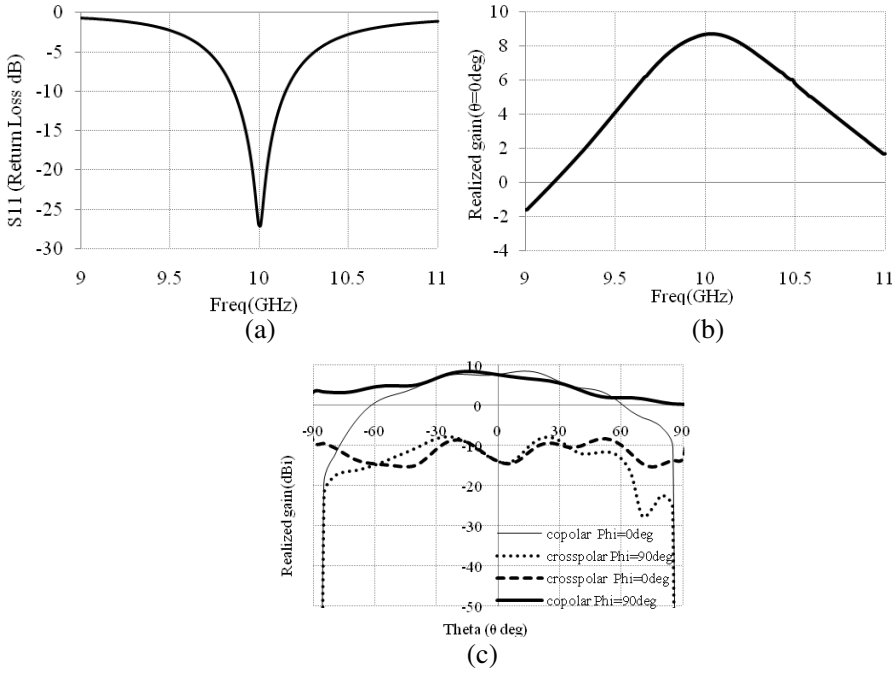

Figure 3. (a) Return loss versus frequency for simple circular patch. (b) Gain versus frequency for simple circular patch. (c) Radiation pattern (co-pol & cross-pol) at 10 GHz for simple circular patch.

$\theta_0 = 0$ or a conical beam $\theta_0 > 0$. The geometrical properties of the FSS control the beamwidth of the radiated beam.

An approximate design equation for the substrate thickness or the gap height in terms of the beam angle is given as

$$k_0 L = \frac{\pi}{\sqrt{{n_1}^2 - (\sin\theta_0)^2}} \tag{1}$$

where

$$k_0 = \frac{2\pi}{\lambda_d} \tag{2}$$

$$n_1 = \sqrt{\varepsilon_r \mu_r} \tag{3}$$

ε_r = Permittivity of the substrate filling the gap

μ_r = Permeability of the substrate filling the gap

L is the height of substrate filling the gap

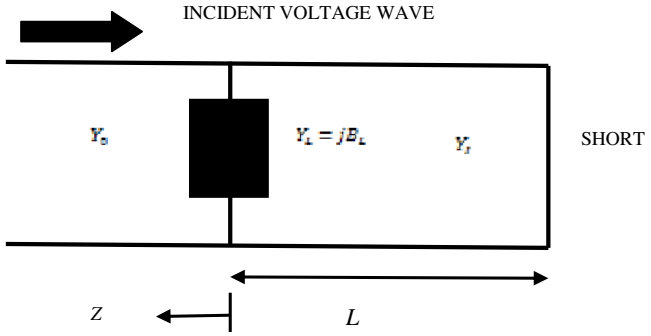

Figure 4. TEN model for disc type FSS structure for far field calculation.

For the present case the substrate is taken as air and hence $\varepsilon_r = 1$, $\mu_r = 1$. The FSS structure can be designed to use higher order parallel plate modes instead of the $n = 1$ modes for which the numerator in (1) is replaced by $n\pi$. This leads to a thicker air gap, and hence affects the low profile structure of CRA which is undesirable and therefore only $n = 1$ case is assumed.

A transmission-line model for the presented CRA structure can be used to derive simple approximate formulas for the radiation pattern of the FSS structure. The transmission line model of the structure under plane-wave illumination is called the transverse equivalent network (TEN), as shown in Fig. 4. The voltage in the TEN models transverse electric field and the current models transverse magnetic field. The shunt susceptance B_L in Fig. 4 models the FSS superstrate, assuming a planar FSS as in the proposed case. The shunt susceptance B_L in the TEN model is equal to the sheet susceptance of the planar FSS (with the sheet admittance of the FSS defined as the ratio of the transverse electric field to the equivalent surface current flowing on the planar FSS for the fundamental Fig. 8: TEN model for FSS structure for calculation of the far field pattern Floquet wave). For the periodic FSS structures the far-field pattern from the TEN analysis is known in closed form once the value of B_L is known. However, determining $B_L(\theta, \phi)$ requires the numerical solution of a periodic structure illuminated by a plane wave [8, 9].

For an HED source located at a height of h_s above the ground plane, the far field from the TEN model is given by [16]

$$E_\theta(r, \theta, \phi) = \left(\frac{-j\omega\mu_0}{4\pi r}\right) E^{-jk_0 r} \cos\phi \cos\theta \times \frac{2Y_0{}^{\mathrm{TM}}}{Y_0{}^{\mathrm{TM}} + j(\mathrm{B}_L - Y_1{}^{\mathrm{TM}} \cot k_{z1} L} \times \frac{\sin k_{z1} h_s}{\sin k_{z1} L} \quad (4)$$

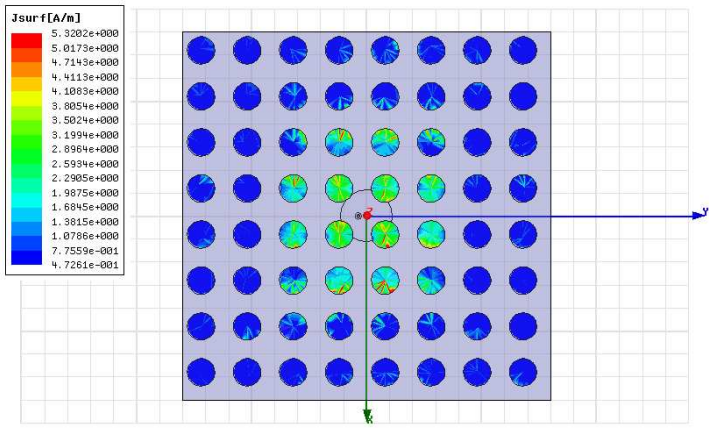

Figure 5. Surface current density on circular disc structures.

$$E_\phi(r,\theta,\phi) = \left(\frac{\mathrm{j}\omega\mu_0}{4\pi r}\right) E^{-jk_0 r}\sin\phi \times \frac{2{Y_0}^{\mathrm{TE}}}{{Y_0}^{\mathrm{TE}} + j(\mathrm{B}_L - {Y_1}^{\mathrm{TE}}\cot k_{z1}L)} \times \frac{\sin k_{z1}h_s}{\sin k_{z1}L} \quad (5)$$

Using the radiation formulas (4) and (5), it is possible to derive formulas for the important radiation characteristics of the antenna. This includes the peak field level radiated at the beam peak, the pattern beamwidth, and the pattern bandwidth [17]. All of these quantities depend on the value of B_L. From the beamwidth, an approximate expression for the directivity can be obtained in the case of a broadside pencil beam, since directivity for a pencil beam is approximately related to the E- and H-plane half-power beamwidths (angle in radians between the 3-dB points) as [18, 19].

$$D = \frac{\pi^2}{\Delta\theta_E \Delta\theta_h} \quad (6)$$

The pattern bandwidth is defined here as

$$BW = \frac{f_2 - f_1}{f_0} \quad (7)$$

where f_0 corresponds to the design frequency and the frequencies f_1 and f_2 are the lower and upper frequencies at which the power density radiated in the direction of angle θ_0 has dropped by a factor of one half (i.e., $-3\,\mathrm{dB}$) from the level at f_0.

The plot of surface current density on the disc type FSS using Ansoft HFSS vs11 is shown in Fig. 5. As it is seen this current is

tapered toward the edges of the cavity. For our design the surface current at the edges of the FSS is about 0.1 of its maximum which is in the middle of the FSS. Therefore, the dimensions of the FSS superstrate layer must be chosen such that, the reflected wave from these edges of FSS can be neglected. Field amplitude and phase depend on dimensions and spacing between parasitic circular shape patches on the dielectric slab. High-gain broadside radiation can be achieved if the elements are fed in phase and current induced at patches are in phase the elements are positioned at different location and at different distance from feed patch (FP). Hence, feed to each disc involves amplitude tapering and phase delay. The amplitude tapering results in decrease in gain but it improves side lobe level (SLL).

The property of the circular patch type FSS and its affect on the performance on the antenna depends on the various parameters of the FSS structure. The parameters are dielectric constant and the thickness of the superstrate on which the circular patch are photo-etched. The FSS circular patch radius and spacing can control the directivity and affect the far fields. The last parameter taken into account is the air spacing (L) between the source and the superstrate. The superstrate is placed at the line of far field and above to get the best performance. The explanation of the results is as given as follows.

3.2.1. Variation in the Dielectric Constant of the Superstrate

The Fig. 6 shows the return loss plots for variation in the dielectric constant of the dielectric used to support the FSS superstrate. The curves are compared together with probe fed circular patch without the FSS superstrate. The superstrate are all forms of Rogers RT Duroid with dielectric constant of $\varepsilon_{r2} = 2.2$, 6.15 and 10.2. Fig. 5 shows that there is approximately no shift in the resonant frequency of operation which is desirable. Though it has been found that the presence of superstrate of different dielectric affect the input impedance and hence the matching of the excitation source. These results are for a single fixed position of the probe. The matching can be improved by moving the probe to achieve optimum matching for wide range of frequencies. There has also been an improvement in the impedance bandwidth of the antenna which is improved from 2.8% for a simple patch to a maximum of 4.02% for a superstrate with a dielectric constant of 10.2. The thickness of all the superstrate is chosen very small, i.e., 0.254 mm ($0.008\lambda_0$).

Gain versus frequency plots are shown in Fig. 7. Gain enhancement with increase in the dielectric constant of the superstrate has been observed. The gain bandwidth is 7.8% and does not considerably reduce as seen in [7] and is about 8.5 % for 10.2 dielectric

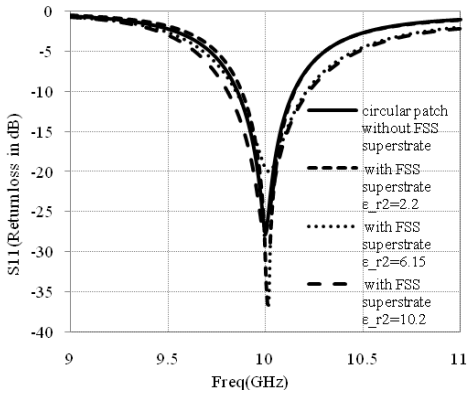

Figure 6. Return loss versus frequency for variation of dielectric constant of FSS superstrate.

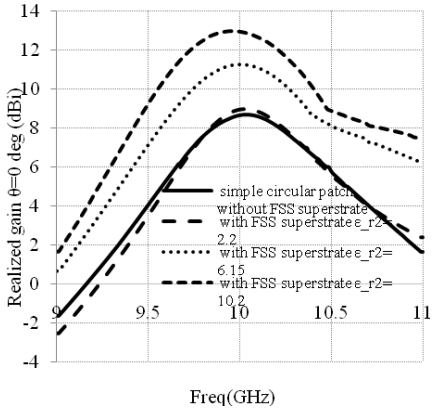

Figure 7. Gain versus frequency for variation in dielectric constant of FSS superstrate. ($\varepsilon_{r1} = 2.2$, $h_1 = 0.762\,\text{mm}$, $h_2 = 0.254\,\text{mm}$, $\varepsilon_r = \mu_r = 1$ (air), $L = 16\,\text{mm}$, $r = 3\,\text{mm}$, $d = 10\,\text{mm}$).

superstrate. Gain improvement of 4.33 dBi for the superstrate having dielectric constant of 10.2 over the conventional simple patch has been achieved. As the superstrate permittivity increases the beam becomes narrower with increase in directivity. This is because for a broadside beam, the complex wave numbers of the two leaky modes (TM_z and TE_z) are usually quite close and become even closer for increased superstrate permittivity.

Figures 8(a)–(c) shows the co-polar and cross polar radiation patterns. The co-polar plot shows the radiation in the broadside

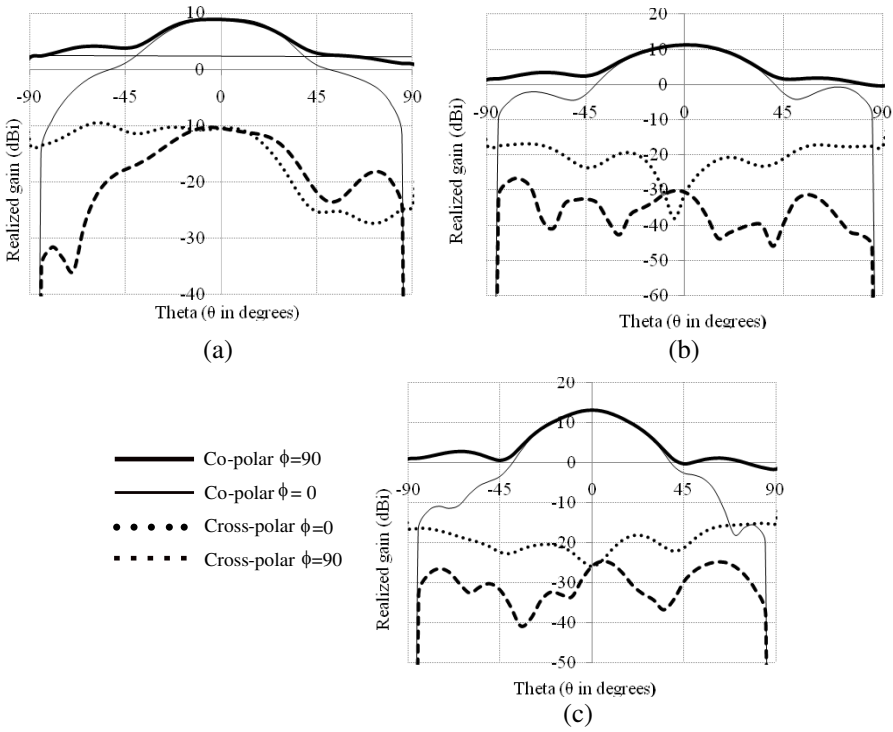

Figure 8. Radiation pattern with FSS superstrate. (a) $\varepsilon_{r2} = 2.2$. (b) $\varepsilon_{r2} = 6.15$. (c) $\varepsilon_{r2} = 10.2$. ($\varepsilon_{r1} = 2.2$, $h_1 = 0.762\,\text{mm}$, $h_2 = 0.254\,\text{mm}$, $\varepsilon_r = \mu_r = 1\,(\text{air})$, $L = 16\,\text{mm}$, $r = 3\,\text{mm}$, $d = 10\,\text{mm}$).

direction with no distortion. The cross-polar level is also improved as compared to that of the original antenna structure without the FSS superstrate loading. The beam is thus a symmetric pencil beam with nearly equal beam widths in the E- and H-plane. The cross polar level in the E- and H-plane also improves considerably for increase in the superstrate permittivity.

3.2.2. Variation in the Thickness of the Superstrate

The thickness of the superstrate also affects the antenna performance without affecting the resonant frequency of operation. As superstrate thickness is increased there is an increase in the gain in the boresight direction. This is clearly observed in the gain versus frequency graph for different superstrate thickness h_2 of RT duroid 5880 (tm) of dielectric constant 2.2 as shown in Fig. 9. The gain is improved

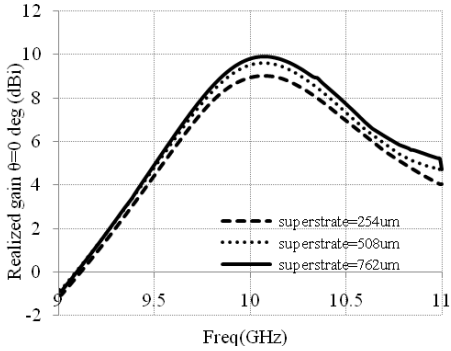

Figure 9. Gain versus frequency for variation in thickness of FSS superstrate. $\varepsilon_{r1} = 2.2$, $h_1 = 0.762\,\text{mm}$, $\varepsilon_{r2} = 2.2$, $\varepsilon_r = \mu_r = 1\,(\text{air})$, $L = 16\,\text{mm}$, $r = 3\,\text{mm}$, $d = 10\,\text{mm}$.

approximately by 1 dB for small change in the thickness of superstrate from 0.254 mm ($0.008\lambda_0$) to 0.762 mm ($0.025\lambda_0$). The simulations present here are according to the substrate available in the laboratory. The simulations have also been performed using FR-4 epoxy of thickness 1.6 mm ($0.05\lambda_0$) as superstrate. This enhances the gain to around 16 dBi approximately doubling the gain for a double increase in dielectric constant and six times increase in the thickness of the superstrate. This is achieved in the measured results.

3.2.3. Variation in the Dimension and Spacing of Circular Disc in FSS Structure

Doubling the gain of the antenna by using FR-4 (1.6 mm) as dielectric support for FSS superstrate has been discussed in the previous section. However, to obtain very thin and low profile compact structure with the acceptable value of the gain enhancement, the parametric study is done on the geometrical properties of disc type FSS with 10 mil thickness as dielectric support.

Figure 10 shows return loss versus frequency for different disc radius, it shows that the antenna resonates at around 10 GHz and there is around 1–2% variation from the centre frequency for change in the disc radius from 1 mm to 4 mm ($0.03\lambda_0$ to $0.13\lambda_0$). Thus the size of the FSS disc does not have much effect on the resonant frequency of operation of the antenna and neither on the impedance bandwidth which remains nearly constant around 2.8%. There is change in the impedance matching which can be improved by changing the probe position for optimum matching conditions. In all the cases the centre

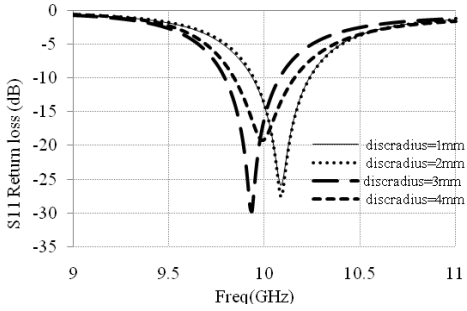

Figure 10. Return loss versus frequency for variation of disc radius (r) of FSS superstrate. $\varepsilon_{r1} = 2.2$, $h_1 = 0.762\,\text{mm}$, $\varepsilon_{r2} = 2.2$, $h_2 = 0.254\,\text{mm}$, $\varepsilon_r = \mu_r = 1\,(\text{air})$, $L = 16\,\text{mm}$, $d = 10\,\text{mm}$.

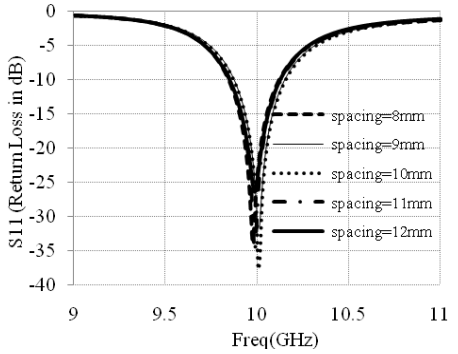

Figure 11. Return loss versus frequency for variation of spacing (d) of FSS superstrate. $\varepsilon_{r1} = 2.2$, $h_1 = 0.762\,\text{mm}$, $\varepsilon_{r2} = 2.2$, $h_2 = 0.254\,\text{mm}$, $\varepsilon_r = \mu_r = 1\,(\text{air})$, $L = 16\,\text{mm}$, $r = 3\,\text{mm}$.

to centre spacing between the discs is kept constant at 10 mm. The variation in spacing keeping the radius constant at 3 mm also does not have a significant effect on the antenna operating frequency as shown in the Fig. 11. But a point of interest is the change in the realized gain of the antenna in the boresight direction ($\theta = 0\,\text{deg}$) at the resonant frequency of operation. From the gain versus frequency plot for different disc radius and spacing, Figs. 12 and 13, it is clear that the gain is considerably improved.

Thus it is clear that the gain is increased by 4.2 dBi for change in the disc radius from 1 mm to 4 mm ($0.03\lambda_0$ to $0.13\lambda_0$). For maximum r/d ratio without shorting the disc structure gain can be increased considerably. This can be done either increasing the disc radius 'r' or

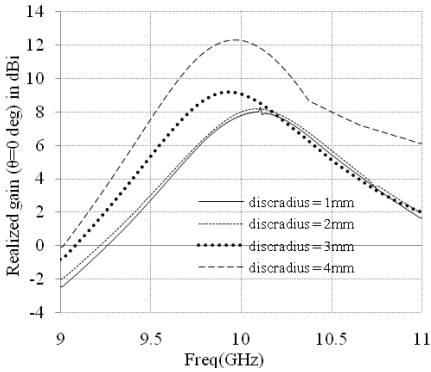

Figure 12. Gain versus frequency for variation in disc radius (r) of FSS superstrate. $\varepsilon_{r1} = 2.2$, $h_1 = 0.762\,\text{mm}$, $\varepsilon_{r2} = 2.2$, $h_2 = 0.254\,\text{mm}$, $\varepsilon_r = \mu_r = 1\,(\text{air})$, $L = 16\,\text{mm}$, $d = 10\,\text{mm}$.

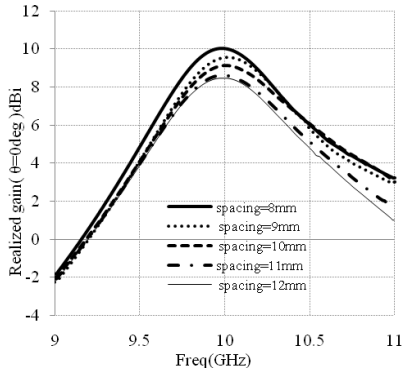

Figure 13. Gain versus frequency for variation in spacing (d) of FSS superstrate. $\varepsilon_{r1} = 2.2$, $h_1 = 0.762\,\text{mm}$, $\varepsilon_{r2} = 2.2$, $h_2 = 0.254\,\text{mm}$, $\varepsilon_r = \mu_r = 1\,(\text{air})$, $L = 16\,\text{mm}$, $r = 3\,\text{mm}$.

decreasing the spacing 'd' in between the discs which again improves the aspect ratio, i.e., r/d ratio. Where r is the radius of the disc and d is the centre to centre spacing between the circular patch type discs.

For closely placed circular discs, FSS acts more like a conducting plate. Equations (8) and (9) shows the -3-dB beam-width in the E- and H-planes. It is seen that the beam-width decreases as B_L increases. The beam-width of a broadside beam varies inversely with B_L. A larger value of B_L means that the FSS superstrate acts more like a conducting plate, confining the fields to the substrate region and allows for less leakage, lowering the attenuation constants of the leaky modes. As the attenuation constants of the leaky modes decrease the effective size of the radiating aperture (where the fields of the leaky modes are significant) increases, narrowing the beam.

$$E \text{ plane} \quad 2\sqrt{\frac{2{n_1}^3}{\pi\overline{B_L}^2}} \tag{8}$$

$$H \text{ plane} \quad 2\sqrt{\frac{2{n_1}^3}{\pi\overline{B_L}^2}} \tag{9}$$

For the case of a FSS superstrate constructed from a periodic structure additional restriction should be placed on the periodicity to avoid having higher order Floquet waves propagate. Only the fundamental (0, 0) Floquet wave should propagate, as this wave is the one that

corresponds to the parallel-plate waveguide mode that is modeled using the TEN of Fig. 8. Higher order Floquet waves that propagate will result in undesirable grating lobes in the radiation pattern. For periods a and b the necessary restriction is [15]

$$d < \frac{\lambda_0}{2}$$

3.2.4. Variation in the Air Gap Height

The air gap between the antenna structure and the patch type FSS superstrate also affect the radiated fields by the antenna. The superstrate should be placed at least at a distance of 'far field' from the antenna structure so that it affects the radiated field and does not affect the near field of antenna radiation.

The shape of the radiation pattern is primarily determined by the air gap or dielectric gap and FSS properties, and only to a minor degree by the type of source for the antennas structure the minimum distance for the radiated far field is given by

$$R > 2D^2/\lambda_0$$

Thus the air gap variation is done for air gap height of 15 mm to 17 mm. The Fig. 12 shows the return loss curves for different air gap heights. The air gap directly controls the beam angle θ and determines whether the beam is a broadside beam or a conical beam. The air gap length (L) is chosen to maintain the radiation in the broadside direction. For a broadside beam the superstrate is placed at an air gap height of about $\lambda/2$.

The frequency of operation is independent of the gap height though it affects the impedance of the antenna structure and hence the matching as shown in Fig. 14.

The Fig. 15 shows the cross polar level variation with the air gap height. From the figure, the sensitiveness of gap height on cross polar level is shown. It can be seen from the figure that the minimum cross polar radiation has been achieved for a gap height of 17 mm in both the E and H planes.

The gain variation with gap height is not significant in the range of 15 mm to 17 mm but decreases considerably after 17 mm as shown in Fig. 16. Thus the gap height of 17 mm gives the optimum gain and cross polar ratio keeping other parameters as constant.

4. EXPERIMENTAL RESULTS

This section presents the measurement results for the prototype fabricated in the laboratory. The measurement of Return Loss has been

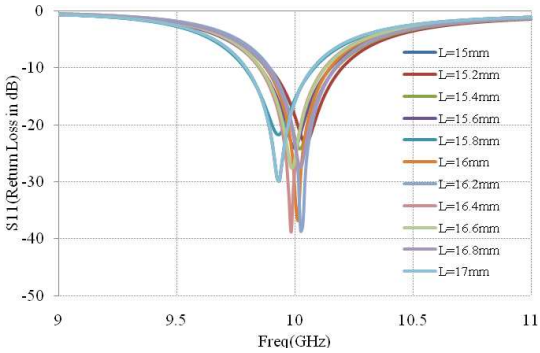

Figure 14. Return loss versus frequency for variation of air gap height (L) of FSS superstrate. $\varepsilon_{r1} = 2.2$, $h_1 = 0.762\,\text{mm}$, $\varepsilon_{r2} = 2.2$, $h_2 = 0.254\,\text{mm}$, $\varepsilon_r = \mu_r = 1\,(\text{air})$, $r = 3\,\text{mm}$, $d = 10\,\text{mm}$.

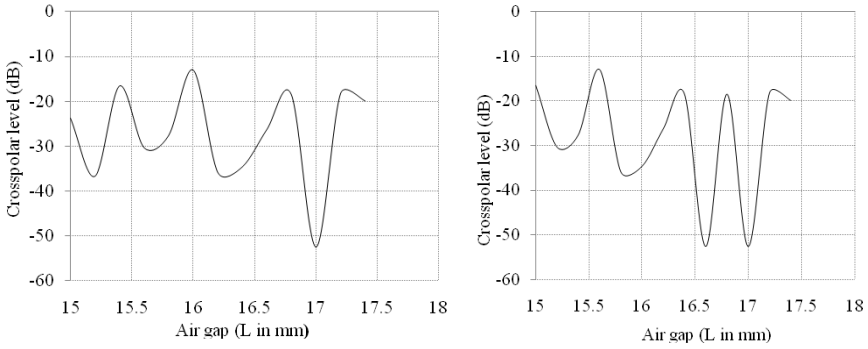

Figure 15. Cross-polar level versus air gap (L) for CRA with disc type FSS superstrate. $\varepsilon_{r1} = 2.2$, $h_1 = 0.762\,\text{mm}$, $\varepsilon_{r2} = 2.2$, $h_2 = 0.254\,\text{mm}$, $\varepsilon_r = \mu_r = 1\,(\text{air})$, $r = 3\,\text{mm}$, $d = 10\,\text{mm}$.

done using Agilent Vector Network Analyzer. The antennas prototypes are shown in Figs. 17(a)–(c). The measured results have been presented for the simple circular patch and CRA with FSS superstrate for selected configurations shown in Fig. 18.

The source antenna consists of a simple circular patch on a 30 mil RT Duroid with $\varepsilon_{r1} = 2.2$. This provides a rigid support for the ground plane, however for production model this can be mounted on an aluminum base plate. The spacing or the height (L) consisting of air gap has been created using Teflon rods for supporting the FSS superstrate. The measurement results confirm that these rods do not affect the antenna performance. Though care has been taken to maintain the accuracy of gap of the superstrate from the patch, there

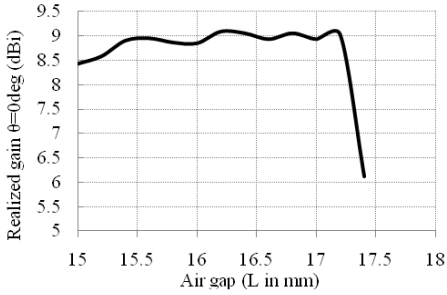

Figure 16. Gain versus air gap (L) for CRA with disc type FSS superstrate. $\varepsilon_{r1} = 2.2$, $h_1 = 0.762\,\text{mm}$, $\varepsilon_{r2} = 2.2$, $h_2 = 0.254\,\text{mm}$, $\varepsilon_r = \mu_r = 1\,(\text{air})$, $r = 3\,\text{mm}$, $d = 10\,\text{mm}$.

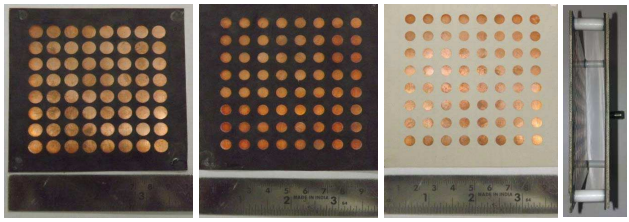

Figure 17. (a) CRA with '$r = 4\,\text{mm}$', '$d = 10\,\text{mm}$' and '$L = 16\,\text{mm}$' with supporting dielectric of FSS superstrate, RT duroid, $\varepsilon_{r2} = 2.2$. (b) CRA with '$r = 3\,\text{mm}$', '$d = 10\,\text{mm}$' and '$L = 16\,\text{mm}$' with supporting dielectric of FSS superstrate, RT duroid, $\varepsilon_{r2} = 2.2$. (c) CRA with '$r = 3\,\text{mm}$', '$d = 10\,\text{mm}$' and '$L = 16\,\text{mm}$' with supporting dielectric of FSS superstrate, RT duroid, $\varepsilon_{r2} = 10.2$. (d) Assembled view [for supporting the RT Duroid substrate a thin frame of FR4 (just at the boundary) has been used].

occurred certain error as the gap setting was done manually which lacked precision and due to very thin superstrate of $h_2 = 10\,\text{mil}$, it was difficult to maintain absolute flatness of the surface. Thus the measurement for radiation pattern has been done only for gap lengths of $L = 16\,\text{mm}$. For production model the superstrate layer can be attached to a thin layer of Styrofoam with $\varepsilon_r = 1.03$. However the return loss curves have been presented for $L = 16\,\text{mm}$.

Measurement results for simple patch are shown in Fig. 18. Fig. 18(a) shows the measured Return Loss versus frequency. The resonant frequency for simple circular patch is 9.82 GHz as compared to the simulation results of 9.97 GHz. Similarly it can be seen for the CRA with FSS superstrate. There is a mismatch of around 1.8% in

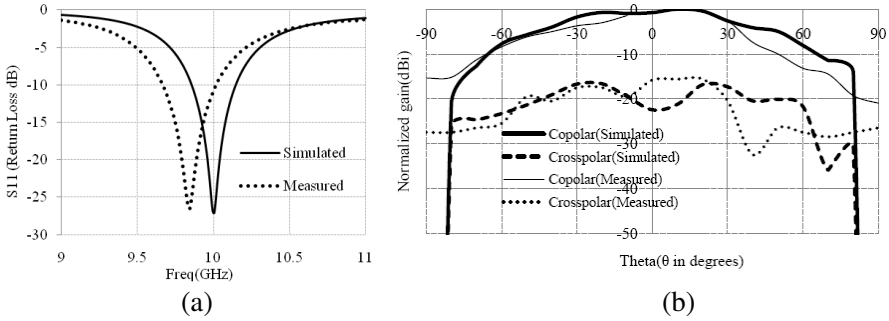

Figure 18. Measurement results for simple patch. (a) Return loss versus frequency. (b) Radiation pattern in E-plane at 9.84 GHz.

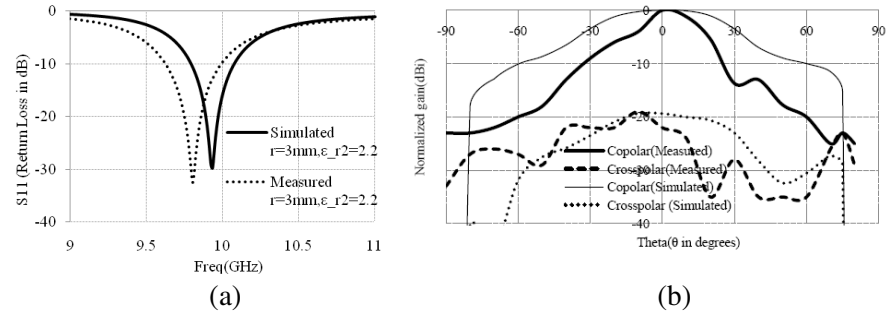

Figure 19. Measurement results for CRA with FSS superstrate. (a) Return loss versus frequency. (b) Radiation pattern in E-plane at 9.80 GHz. $\varepsilon_{r1} = 2.2$, $h_1 = 0.762$ mm, $\varepsilon_{r2} = 2.2$, $h_2 = 0.254$ mm, $\varepsilon_r = \mu_r = 1$ (air), $L = 16$ mm, $r = 3$ mm, $d = 10$ mm.

the resonant frequencies which can be attributed to the fabrication and measurement errors. The radiation pattern measurement has been done for only the E-plane of the antenna. Fig. 18(b) shows the Radiation pattern in E-plane at 9.84 GHz. The normalized gain pattern is measured and it is clear that they are consistent with the simulation results shown in Fig. 3(c) and Fig. 8(a), respectively.

Measurement results for CRA with FSS superstrate $L = 16$ mm, $\epsilon_{r2} = 2.2$, $r = 3$ mm are given in Fig. 19. Fig. 19(a) shows the Return Loss with frequency for $L = 16$ mm. The measured resonant frequency 9.76 GHz whereas the simulated is at 10 GHz, the mismatch can be attributed to the fabrication and measurement errors. Fig. 19(b) show the E-plane radiation pattern.

Measurement results for CRA with FSS superstrate $L = 16$ mm, $\epsilon_{r2} = 10.2$, $r = 3$ mm are given in Fig. 20. The explanations for the

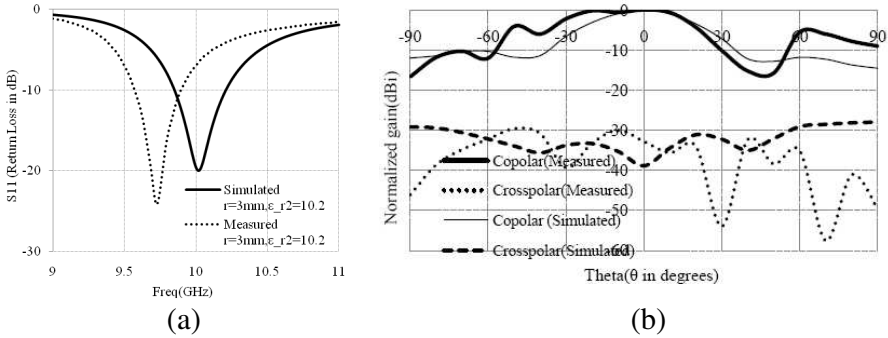

(a) (b)

Figure 20. Measurement results for CRA with FSS superstrate. (a) Return loss versus frequency. (b) Radiation pattern in E-plane at 9.71 GHz. $\varepsilon_{r1} = 2.2$, $h_1 = 0.762\,\text{mm}$, $\varepsilon_{r2} = 10.2$, $h_2 = 0.254\,\text{mm}$, $\varepsilon_r = \mu_r = 1\,(\text{air})$, $L = 16\,\text{mm}$, $r = 3\,\text{mm}$, $d = 10\,\text{mm}$.

graphs have already been provided in the section of Full Wave analysis. However it can be seen that there is a degradation in the copolar pattern with increased dielectric constant value of the superstrate, though it minimizes the crosspolar level. This trade off characterstic puts a limit to the use of superstrates with higher dielectric constants above a certain value. The measurement results are in good agreement to the simulation results.

5. CONCLUSION

The cavity reflex antenna employing circular patch type FSS superstrate were designed, simulated and fabricated. Equal E and H-plane radiation were achieved for suggested FSS superstrate configuration. Cross polar variation with the air gap were studied. The results reveals that the cross polar level is very sensitive with the air gap height. Whereas, it was also found that resonant frequency and input impedance are less sensitive. A parametric study was conducted on the size and spacing of the circular patch type FSS. Its effect on the copular and crosspolar field is provided. Moreover, gain versus frequency plots were given for the various configurations. The antenna was fabricated and successfully tested. The results are in good agreement. For the frequency range where the reflection coefficient of surface is about unit, the radiating source and the superstrate layer produce resonance condition in which the directivity of the antenna increases considerably and hence can be employed for UWB antennas also for improved directivity over the whole bandwidth.

REFERENCES

1. Jackson, D. and N. Alexopoulos, "Gain enhancement methods for printed circuit antennas," *IEEE Trans. on Antennas and Propag.*, Vol. 33, No. 9, 976–987, Sep. 1985.
2. Alexopoulos, N. G. and D. R. Jackson, "Fundamental superstrate (cover) effects on printed circuit antennas," *IEEE Trans. on Antennas and Propag.*, Vol. 32, 807–816, Aug. 1984.
3. Vettikalladi, H., O. Lafond, and M. Himdi, "High-efficient and high gain superstrate antenna for 60-GHz indoor communication," *IEEE Antenna Wireless Propag. Lett.*, Vol. 8, 1422–1425, 2009.
4. Lee, Y. J., J. Yeo, R. Mittra, and W. S. Park, "Application of electromagnetic bandgap (EBG) superstrates with controllable defects for a class of patch antennas as spatial angular filters," *IIEEE Trans. on Antennas and Propag.*, Vol. 53, No. 1, 224–235, Jan. 2005.
5. Attia, H., L. Yousefi, M. M. Bait-Suwailam, M. S. Boybay, and O. M.Ramahi, "Enhanced-gain microstrip antenna using engineered magnetic superstrates," *IEEE Antenna Wireless Propag. Lett.*, Vol. 8, 1198–1201, 2009.
6. Munk, B. A., *Frequency Selective Surfaces: Theory and Design*, Wiley, New York, 2000.
7. Foroozesh, A. and L. Shafai, "Investigation into the effects of the patch type FSS superstrate on the high-gain cavity resonance antenna design," *IEEE Trans. on Antennas and Propag.*, Vol. 58, No. 2, 258–270, Feb. 2010.
8. Zhao, T., D. R. Jackson, J. T.Williams, H. Y. Yang, and A. A. Oliner, "2-D periodic leaky-wave antennas — Part I: Metal patch design," *IEEE Trans. on Antennas and Propag.*, Vol. 53, 3505–3514, Nov. 2005
9. Zhao, T., D. R. Jackson, and J. T. Williams, "2-D periodic leaky-wave antennas — Part II: Slot design," *IEEE Trans. on Antennas and Propag.*, Vol. 53, 3515–3524, Nov. 2005.
10. S. Maci, M. Caiazzo, A. Cucini, and M. Casaletti, "A pole-zero matching method for EBG surfaces composed of a dipole FSS printed on a grounded dielectric slab," *IEEE Trans. on Antennas and Propag.*, Vol. 53, 70–81, Jan. 2005.
11. Foroozesh, A. and L. Shafai, "On the characteristics of highly directive resonant cavity antenna having metal strip grating superstrate," *IEEE Trans. on Antennas and Propag.*, Vol. 60, No. 1, 78–91, Jan. 2012.
12. Vaidya, A. R., R. K. Gupta, S. K. Mishra, and J. Mukherjee,

"Effect of superstrate height on gain of MSA fed fabry perot cavity antenna," *Loughborough Antenna and Propagation Conference*, 2011.

13. Pirhadi, A., "Wideband high directive aperture coupled microstrip antenna design by using a FSS superstrate layer," *IEEE Trans. on Antennas and Propag.*, Vol 60, No. 4, 2101–2106, 2012.
14. Feresidis, A. P. and J. C. Vardaxoglou, "High gain planar antenna using optimized partially reflective surfaces," *IEE Proceedings*, 2001.
15. Feresidis, A. P., S. Wang, and C. Vardaxoglou, "Artificial magnetic conductor surfaces and their application to low profile high gain planar antennas," *IEEE Trans. on Antennas and Propag.*, Vol. 53, No. 1, Jan. 2005.
16. Jackson, D. R., P. Burghignoli, G. Lovat, F. Capolino, J. Chen, D. R. Wilton, and A. A. Oliner, "The fundamental physics of directive beaming at microwave and optical frequency and the role of leaky waves," *Proceedings of the IEEE*, Vol. 99, No. 10, Oct. 2011.
17. Zhao, T., D. R. Jackson, and J. T. Williams, "General formulas for 2D leaky wave antennas," *IEEE Trans. on Antennas and Propag.*, Vol. 53, No. 11, 3525–3533, Nov. 2005.
18. Balanis, C. A., *Antenna Theory: Analysis and Design*, 3rd Edition, Wiley, New York, 2005.
19. Lovat, G., P. Burghignoli, and D. R. Jackson, "Fundamental properties and optimization of broadside radiation from uniform leaky-wave antennas," *IEEE Trans. on Antennas and Propag.*, Vol. 54, No. 5, 1442–1452, May 2006.